Received: 29 November 2017 | Revised: 14 February 2018 | Accepted: 18 March 2018

DOI: 10.1002/jbio.201700359

Journal of BIOPHOTONICS

FULL ARTICLE

Assessing hyperthermia-induced vasodilation in human skin in vivo using optoacoustic mesoscopy

Andrei Berezhnoi[1,2] | Mathias Schwarz[1,2,3] | Andreas Buehler[1,2] | Saak V. Ovsepian[1,2] | Juan Aguirre[1,2] | Vasilis Ntziachristos[1,2*]

[1]Chair of Biological Imaging, Technische Universität München, Munich, Germany

[2]Institute of Biological and Medical Imaging, Helmholtz Zentrum München, Neuherberg, Germany

[3]iThera Medical GmbH, Munich, Germany

*Correspondence
Vasilis Ntziachristos, Chair of Biological Imaging, Technische Universität München, Ismaninger Straße 22, D-81675 Munich, Germany.
Email: v.ntziachristos@tum.de

Funding information
H2020 LEIT Information and Communication Technologies, Grant/Award Number: 687866; H2020 European Research Council, Grant/Award Number: 694968

The aim of this study was to explore the unique imaging abilities of optoacoustic mesoscopy to visualize skin structures and microvasculature with the view of establishing a robust approach for monitoring heat-induced hyperemia in human skin in vivo. Using raster-scan optoacoustic mesoscopy (RSOM), we investigated whether optoacoustic (photoacoustic) mesoscopy can identify changes in skin response to local heating at microvasculature resolution in a cross-sectional fashion through skin in the human forearm. We visualized the heat-induced hyperemia for the first time with single-vessel resolution throughout the whole skin depth. We quantified changes in total blood volume in the skin and their correlation with local heating. In response to local heating, total blood volume increased 1.83- and 1.76-fold, respectively, in the volar and dorsal aspects of forearm skin. We demonstrate RSOM imaging of the dilation of individual vessels in the skin microvasculature, consistent with hyperemic response to heating at the skin surface. Our results demonstrate great potential of RSOM for elucidating the morphology, functional state and reactivity of dermal microvasculature, with implications for diagnostics and disease monitoring. Image: Cross-sectional view of skin microvasculature dilated in response to hyperthermia.

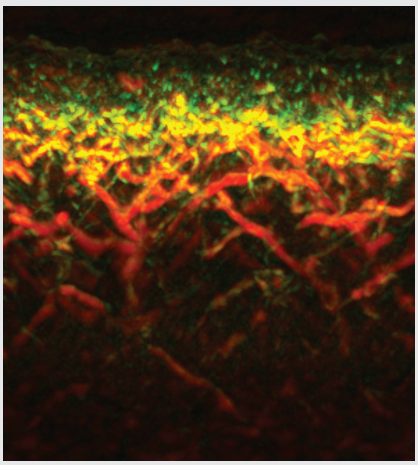

KEYWORDS
hyperemia, induced hyperthermia, optoacoustic techniques, skin, vasodilation

1 | INTRODUCTION

Analysis of skin morphology and microvasculature as well as its response to external stimuli such as heating or pharmacological treatments may reveal vasculature dysfunctions linked to cardiovascular diseases, diabetes, obesity, and metabolic syndrome [1–3]. This is hardly surprising given that the skin, the largest organ of the human body, is regulated by metabolic and homeostatic processes and is systemically affected by various health conditions. For example, obesity and diabetes are associated with abnormalities in the dermal microvascular bed, reflecting poor skin perfusion and impaired endothelial function [4–6]. Congestive heart failure [7, 8], atherosclerosis [9] and metabolic syndrome [10] may

be associated with altered vascular responses, which can be measured as an impairment in heat-induced vasodilation and associated increase in skin perfusion, known as hyperemia [7]. Thus, measuring the vascular response to temperature changes may uncover generalized systemic vasculature dysfunction associated with the progression of different diseases [11, 12], and could provide better cardiovascular risk assessment than the Framingham Risk Score [13].

Optical methods, due to several advantages including portability, easy access and safe use, have been considered for measuring skin perfusion at rest or in response to local heating that induces hyperemia. Laser Doppler flowmetry (LDF) provides relative perfusion measurements detected as Doppler shifts based on dynamic laser light scattering measurements produced by moving red blood cells [14]. LDF has been used to detect hyperemia in human forearm skin locally heated from 35 to 43°C [15, 16], where bulk blood flow could be measured with spatial resolution of approximately 1.0 mm^3. Scanning the laser beam can generate flow imaging by means of laser Doppler perfusion imaging (LDPI) [17], and is shown to enable spatial measurements of skin perfusion associated with thermally induced hyperemia [18]. Alternatively, laser speckle contrast imaging (LSCI) allows acquisition of skin perfusion maps over a large region with higher temporal resolution than LDPI. LSCI is based on the analysis of the fluctuation of the speckle patterns produced by the phase shifts in scattered light caused by moving red blood cells [19]. Intensity of the speckle pattern fluctuates more rapidly in regions of higher blood flow than in regions with lower flow. By acquiring an image of the speckle pattern and quantifying the blurring of the speckles, spatial maps of relative blood flow can be obtained. LDPI and LSCI typically characterize superficial flow as they rely on photons scattered from the surface of the tissue imaged. Nevertheless, it has been reported that the repeatability of blood flow measurements using LPDI or LSCI is poor [17, 18]. Diffuse correlation spectroscopy (DCS) [20] along with its extension for volumentric optical imaging, diffuse correlation tomography (DCT) [21], have also been considered for assessment of local blood flow changes in deep tissue. Like LDPI and LSCI, DCS and DCT derive the blood flow information based on the photons scattered by moving red blood cells and using statistical approaches. However DCS and DCT suffer low SNR and do not provide sufficient resolution to resolve individual deep microvessels, which limits visualization of skin microvasculature [22].

Optoacoustic mesoscopy, in particular raster-scan optoacoustic mesoscopy (RSOM) [23], has shown unique ability to visualize skin morphology, including microvasculature [24, 25], especially when employing ultra-wideband (UWB) ultrasound measurements spanning the range from 20 to 180 MHz [23]. As the largest and highly metabolic organ, the skin receives dense supply of nutrients and oxygen via system of cutaneous microvasculature, which include capillaries, arterioles, met-arterioles, venules and system of micro-anastomoses, known also as thoroughfare channels. In terms of diameter, this system of vessels range from a few microns diameter capillaries to arterioles and venules reaching up to one hundred microns [26]. Quantification of vascular changes allows detection of inflammation associated with psoriasis and eczema [27]. Multispectral RSOM has demonstrated the ability to reveal different natural chromophores in skin, such as melanin, as well as oxygenated and deoxygenated hemoglobin; the technique can also measure blood oxygenation levels in single vessels [28]. RSOM utilizes photon pulses shorter than 10 ns to illuminate the skin followed by capture of optoacoustic waves by raster-scanning a UWB detector in a 2-dimensional pattern parallel to the skin surface. Finally, image reconstruction algorithms are employed to produce 3-dimensional (3D) light absorption maps of skin tissue. The technique visualizes skin to depths of 1-2 mm with resolution that can exceed 10 microns [29].

In this work we considered RSOM as an alternative to optical techniques for imaging human skin responsiveness to local heating. We hypothesized that RSOM could visualize changes in skin microvasculature after local heating, overcoming the poor resolution and superficial imaging performance of optical techniques. Given the ability of RSOM to resolve 3D skin morphology structures, we further postulated that RSOM could lead to comprehensive readings of skin responses to temperature extending beyond the reach of optical imaging, offering precision and reproducibility throughout the entire skin. To examine these hypotheses, we performed RSOM imaging of the human forearm under local heating precisely controlled using a custom-built apparatus, and we examined vascular dilation through the skin depth. We verified the reproducibility of the measurements by exploiting the high resolution offered by RSOM, and we quantified the gradual increase in blood volume in skin with the rise of the skin temperature. Finally, we discuss our findings and illustrate possible uses of RSOM in clinical care and diagnostics.

2 | EXPERIMENTAL

2.1 | Institutional review board

All human experiments were approved by the Ethics Review Board of Helmholtz Zentrum München, and participants provided written informed consent.

2.2 | UWB clinical RSOM system

To investigate perfusion changes in human skin induced by local hyperthermia, we utilized an UWB handheld clinical RSOM system built in-house [24] (see Supplementary Note 1 in Appendix S1), together with a custom-built temperature control system for local heating of the forearm (see below).

2.3 | Temperature control system

In order to induce heat-mediated vasodilation in a controlled fashion, we designed a system for heating the coupling

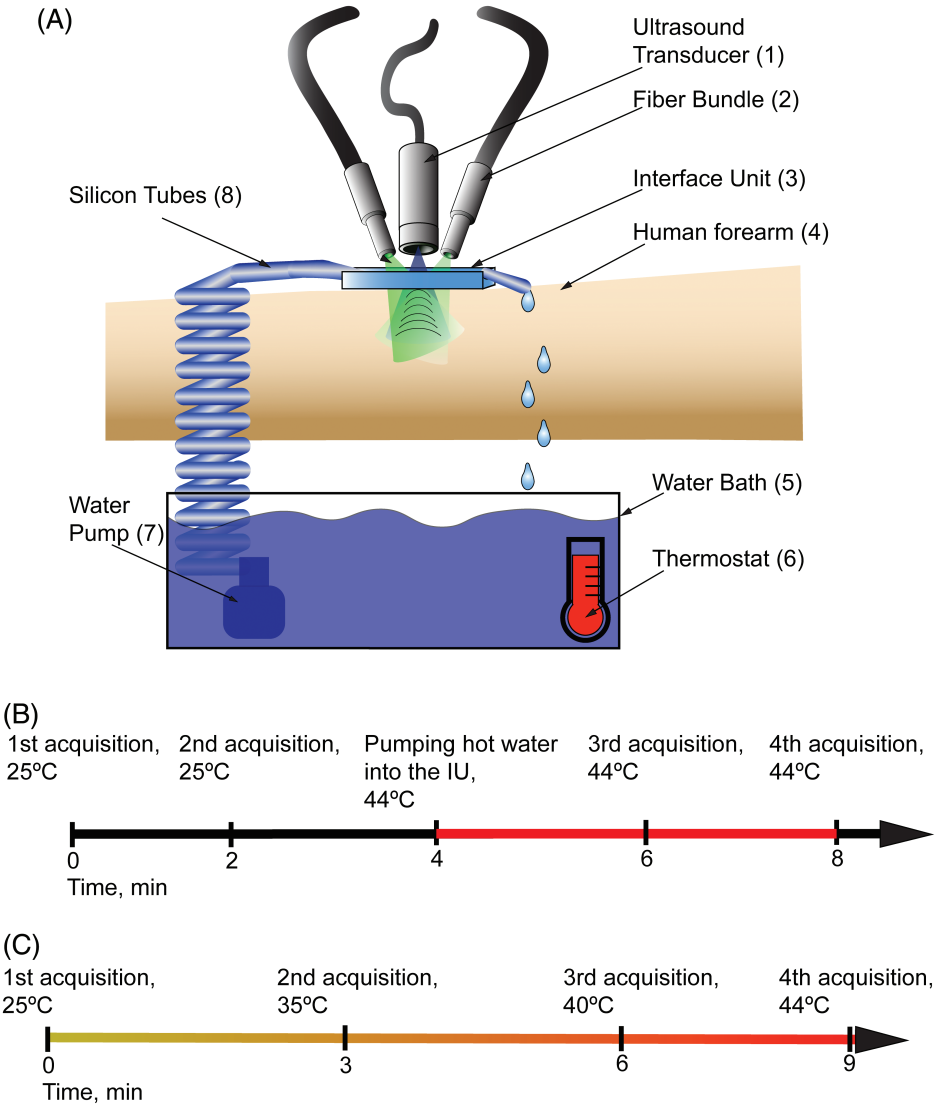

FIGURE 1 Schematic of RSOM system and experimental protocol. (A) Custom-built handheld RSOM system featuring a precise temperature control system for focal heating. The ultrasound transducer (1) and fiber bundles (2) are raster-scanned together over the ROI on the skin surface. The interface unit (3) contains coupling medium and is in direct contact with the forearm (4). Water (5) in a thermostated bath (6) is pumped (7) via silicon tubes (8) through the interface unit. (B) Schematic of the timing of RSOM measurements during rapid heating experiments. The red line indicates a water temperature of 44°C in direct contact with the skin surface. (C) Schematic of the timing of RSOM measurements during gradual heating experiments

medium which is in direct contact with the region of interest (ROI) (Figure 1A). The system can heat the coupling medium from room temperature (25°C) to 50°C with 1°C precision. The thermostat is used to adjust the temperature in the water bath to the desired value, and then the water is pumped into the interface unit. Once the water level in the interface unit reaches a certain height, water drips back into the water bath naturally, without disturbing the subject or interfering with the imaging procedure. This creates a closed loop maintained at the desired temperature.

2.4 | Image reconstruction and representation

Images were reconstructed using a 3D beam-forming algorithm [30] executed on a graphics processing unit to reduce computation time. The synthetic aperture method was implemented in order to take into account the detector's directivity [31]. Prior to reconstruction, data were filtered with a 4th-order exponential filter to divide them into a low-frequency band (10-40 MHz) and high-frequency band (40-120 MHz).

Data were reconstructed in 3D and the maximum intensity projection (MIP) was taken along one of the dimensions. The MIP for the high-frequency band occupied the green channel of an RGB (Red, Green, Blue) image, while the MIP for the low-frequency band occupied the red channel. Following frequency band equalization, smaller vessels appeared in green, while larger vessels appeared in red [27]. The vessels with intermediate diameter appear in different shades of yellow.

2.5 | Experimental procedure

Hyperemic response was measured in 6 healthy, nonsmoking volunteers (1 woman, 5 men; age range, 25-35 years). Volunteers gave written informed consent before participation. To ensure stability of measurements, all participants sat in a chair quietly in the temperature-controlled room for at least 30 minutes before experiments. Hyperemia was analyzed in response to rapid heating, when the temperature of the coupling medium was raised from 25°C to 44°C, and the ROI was imaged before and after heating. Hyperemia was also analyzed in response to gradual heating, when the temperature of the coupling medium was raised gradually from

25°C to 44°C, and the ROI was imaged several times during heating.

2.5.1 | Rapid heating

For each volunteer, 1 set of measurements was acquired on the dorsal and volar aspects of the forearm, approximately 10 to 15 cm away from the wrist. Each set of measurements consisted of 2 data acquisitions before local heating and 2 acquisitions after. Acquisitions followed the timeline shown in Figure 1B. All acquisitions involved the same skin area, with the interface unit remaining affixed to the forearm throughout the experiment. In order to avoid blood volume variations caused by vascular heterogeneity in the skin, rigid image registration was performed between the images taken before and after heating. Fiducial markers (small ink dot on the skin surface) or the vasculature network were used as a reference for image registration. Partial blood volume (PBV) and single vessel diameters were calculated from the reconstructed 3D images (see below).

2.5.2 | Gradual heating

Data were acquired at several temperatures of coupling medium (25°C, 35°C, 40°C, 44°C) in 3 volunteers. The temperature was controlled constantly in the water bath and the compartment of the unit interface, and it remained constant during acquisition. The interface unit was attached to a volar aspect of the forearm in the same manner as for rapid heating measurements. Data were acquired at 3-minute intervals to ensure the stability of the coupling medium temperature (Figure 1C). PBV was calculated at each temperature.

2.6 | Calculation of perfusion-related vascular parameters

2.6.1 | Partial blood volume

To quantify the blood volume in the skin, we defined an ROI to be a volume of approximately 4 mm (x) by 2 mm (y) by 0.75 mm (z) lying below the epidermal-dermal junction. ROI size differed slightly among volunteers because of motion and skin depth variations. Total blood volume (TBV) was calculated by applying a threshold corresponding to 20% of the maximum intensity. All voxel values below this threshold were set to 0, while all voxel values above the threshold were set to 1. Then, $TBV = \sum V_i \times dV$, where V_i is the value of voxel i and dV is the voxel volume. To avoid intersubject variation in skin blood volume, PBV was calculated for each participant (PBV_k) using the following formula: $PBV_k = TBV_k/Vol_k$, where Vol_k is the ROI volume. Mean PBV and its SD were calculated at each temperature. Differences between sets of measurements were assessed for significance using a Student's paired-samples t test.

2.6.2 | Vessel diameter

Vessel diameter was calculated from a cross-sectional MIP of the reconstructed images converted in gray colormaps.

Blood vessels of various diameters from 6 volunteers were selected randomly from the horizontal plexus area for analysis by an independent observer in the reconstructed image corresponding to the 1st acquisition. The same set of vessels was followed throughout the rest of the reconstructed images. Vessels which disappeared from the field-of-view due to motion or because they lay underneath dilated microvasculature were excluded from the analysis.

Diameter was defined as the full-width half maximum obtained from a profile of a vessel in the direction of its radius, which assumes that vessels can locally be considered cylinders.

3 | RESULTS

3.1 | Imaging heat-induced vasodilation

We investigated whether RSOM could image the effects of local hyperthermia on cutaneous microvasculature on the volar and dorsal aspects of the forearm of 6 healthy volunteers. Both aspects were imaged at room temperature (baseline) for 2 minutes. Then, each aspect was heated locally to 44°C at the skin surface starting at $t = 4$ minutes (see Methods, Figure 1B). To observe the response of the vascular bed to heating, the optoacoustic images were acquired at $t = 6$ and 8 minutes.

Figure 2A-H shows typical RSOM images of the dorsal skin (Fig. 2A-D) and the volar skin (Fig. 2E-H) before and after heating. In Figure 2A, the epidermal layer (labeled "1") is visible atop a vascular network in the horizontal plexus (labeled "2"). The anatomical structure of skin in Figure 2 is consistent with the structure seen in previous RSOM studies [24]. Figure 1 also shows typical RSOM images of the volar skin before heating (Figure 2E,F) and after heating (Figure 2E,F). The layered structure of skin is less evident in the volar aspect than the dorsal aspect because of the lower amount of melanin in the volar part. The bright yellow point marked with an arrow in Figure 2E-H is a fiducial ink signal used to perform image registration, since this point shifted slightly from image to image because of participant motion. The images indicate that upon heating of the skin, vascular density increased throughout the measured depth, and the signal in deep layers shifted to lower frequencies (red color), reflecting vasodilation.

Next we quantified the heat-induced vasodilation in skin by measuring the diameters of individual vessels before and after heating (Figure 2I,J). Figure 2K depicts the signal intensity profile change of a single vessel, indicating approximately 57% diameter increase in response to local hyperthermia.

3.2 | Quantitation of vascular response to rapid heating

3.2.1 | Blood volume

To further demonstrate the ability of RSOM to measure effects of thermal stimulation on perfusion and blood supply

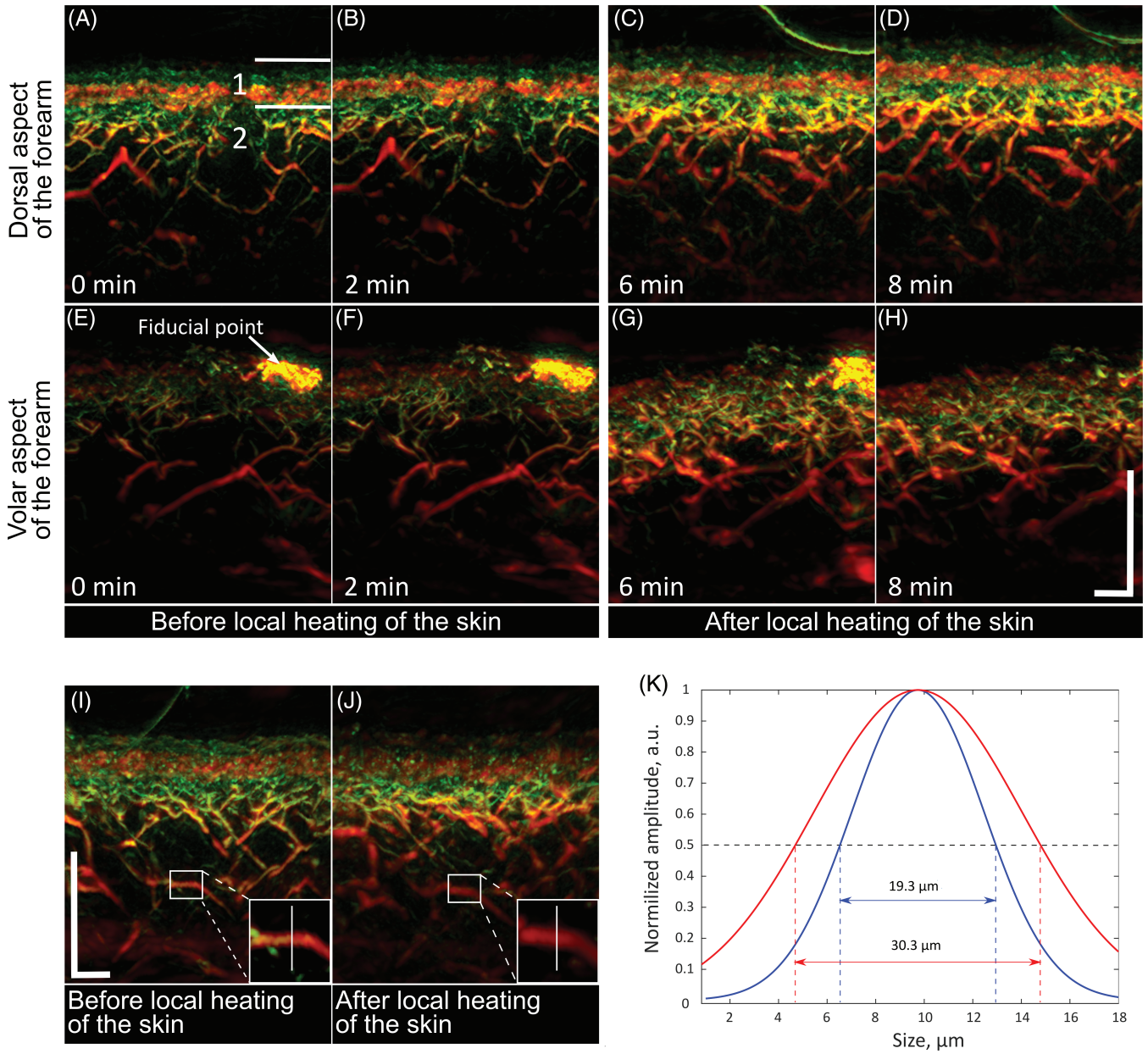

FIGURE 2 RSOM imaging of heat-induced dermal vasodilation. The forearm of a healthy volunteer was imaged before and after heating at 44°C. (A-D) Sagittal views of the dorsal aspect of the forearm before and after heating. In panel (A), horizontal lines demarcate the epidermis (1) and dermis (2), (E-H) sagittal views of the volar aspect of the forearm before and after heating, (I and J) sagittal view of the volar aspect of the forearm showing the dilation of a single vessel (boxed) before and after heating. Inset, close-up view of the vessel, with the vertical line indicating the cross-section displayed in panel (K) and (K) Amplitude profile of the vessel in panels (I) and (J), before (blue) and after (red) heating. Scale bars, 500 µm

in skin, we quantified blood volume before and during focal heating (see Methods) from the data described above.

Figure 3 depicts quantitative parameters of the blood volume and vasodilation in the dermis of volar (Figure 3A) and dorsal (Figure 3B) aspects of the forearm before heating (white bars) and during heating (gray bars). Average PBV in the skin of the volar aspect of the forearm before heating was 2.61% ± 0.61% at $t = 0$ minutes and 2.46% ±0.56% at $t = 2$ minutes. During local heating, the PBV increased significantly and plateaued at a level twice as high as before heating, with average PBV reaching 4.63% ±1.10% at $t = 6$ minutes and 4.66% ±1.00% at $t = 8$ minutes (Figure 3A). Baseline blood volume in the dorsal aspect was 2.70% ± 0.41% at $t = 0$ minutes and 2.89% ± 0.18% at $t = 2$ minutes (similar to the corresponding values in the volar aspect), and it increased significantly to 4.44% ± 0.86% at $t = 6$ minutes and 5.40% ± 0.86% at $t = 8$ minutes (Figure 3B). These changes in blood volume correspond to increases of 1.83-fold (volar) and 1.76-fold (dorsal) over baseline.

3.2.2 | Single vessel dilation

Figure 3C shows the change in diameter of 12 arbitrarily selected blood vessels from the dermal upper plexus of the

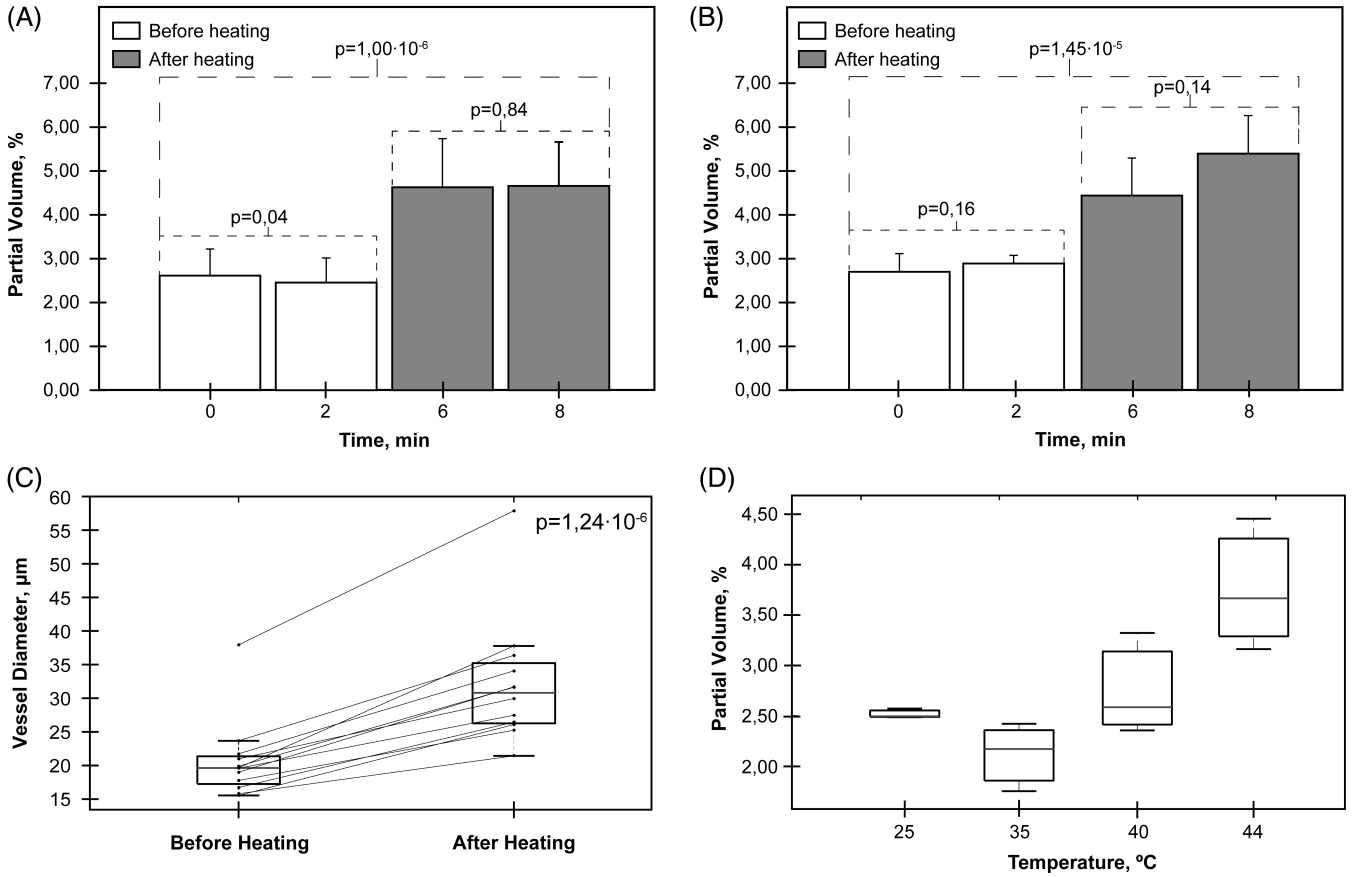

FIGURE 3 RSOM quantification of heat-induced vasodilation. (A and B) The volar and dorsal aspects of the forearms of 6 healthy volunteers were imaged using RSOM before and after heating at 44°C. PBV was measured in dermis of the (A) volar aspect and (B) dorsal aspect, (C) blood vessel diameter was measured in 12 arbitrarily selected vessels in the dermal upper plexus of the volar forearm of multiple volunteers. Solid black lines connect diameters of the same vessel before and after heating, (D) PBV was measured in dermis while the temperature of the coupling medium at the skin surface of 3 volunteers was gradually heated from 25°C to 44°C over 9 minutes. *P* values indicate the differences between selected samples

volar aspect of the forearm. Median diameter was 19.3 µm before heating and 30.8 µm after heating, corresponding to a median increase of 63% (interquartile range, 30%) across all 12 vessels measured. Given the quadratic dependence of volume on radius, a 63% increase in diameter corresponds to a 2.4-fold increase in blood volume, comparable to the 1.83-fold increase obtained in the previous experiments (Figure 3A,B). Given the quartic dependence of blood flow on vessel radius (Poiseuille's law), this increase in radius corresponds to an approximately 6-fold increase in blood flow.

3.3 | Quantitation of vascular response to gradual heating

To explore the temporal resolution of the technique in greater detail, we investigated whether it could capture changes in vascular morphology in response to gradual local heating. RSOM was used to image the volar aspect of 3 healthy volunteers over 9 minutes as the coupling medium was gradually heated from 25°C to 44°C. RSOM images were recorded every 3 minutes, and PBV in the dermis was calculated. Figure 3D shows that in all 3 volunteers, blood volume decreased as temperature increased from 25°C to 35°C and then increased with heating from 35°C to 44°C. As a result, blood volume at 44°C was approximately 1.5-fold greater than the volume at 25°C.

4 | DISCUSSION AND CONCLUSION

Here we demonstrate the capability of RSOM for detailed, cross-sectional visualization of microvascular changes in the skin in the volar and dorsal aspects of the human forearm in response to local hyperthermia. Dermal blood volume and vasodilation were quantitated based on single-wavelength images obtained at 532 nm. Heating the skin to 44°C for 4 minutes increased the diameter of individual vessels as much as 1.56-fold, increasing blood volume in the skin by 2- to 3-fold. To the best of our knowledge, this is the first report of the effects of hyperthermia on dermal microvasculature at the resolution of single microvessels through the entire skin depth.

The heat-induced increase in blood volume of the skin observed here with RSOM confirms results obtained using purely optical imaging techniques [15, 16], where the blood volumes increase 2- to 4-fold over the time span used in this study. However, our technique goes substantially further than purely optical techniques by allowing the analysis of hyperemia at the level of single vessels. This ability may be valuable for elucidating the poorly understood process of vasodilation and vascular recruitment in nonglabrous skin exposed to focal hyperthermia [16] or other physiological and pharmacological interventions. Heat-induced vasodilation may involve several steps: an early phase of dilation, which peaks after 2 to 3 minutes, is followed by an intermediate phase when blood flow plateaus [16], after which it gradually tapers back to the preheating baseline in the late "die away" phase when heating has continued for approximately 40 minutes [32]. The present study looked only at a few time points after heating, so our results likely reflect the early phase of vasodilation. Remarkably, we were able to capture the gradual increase in blood volume with gradually increasing temperature for 9 minutes, suggesting that our system will be useful for analyzing earlier and later stages of the vasodilation process. This may provide a useful read-out for basic and clinical research into vascular function, since early stages of vasodilation are thought to reflect a fast neural response involving the axon reflex, while later stages reflect a slower response involving release of neuromediators and vasodilators such as nitric oxide [33]. The initial increase in the blood volume, possibly due to mild local cooling (Figure 3D) of the skin surface at 25°C, is likely to result from so called cold vasodilation, a transient dilation response of small blood vessels exposed to cold, as reported elsewhere [16]. The "cold vasodilation" has been observed in glabrous skin where it is largely attributable to anastomoses effect. In nonglaborus skin, which is found in forearm, the "cold vasodilation" effect might be linked to relaxation and dilation of capillaries resulting in the slight increase of the blood volume. These effects, however, require further investigation to improve our understanding of the thermoregulatory function of skin.

For these experiments, we custom designed a temperature control system that can induce hyperthermia locally and should easily be accommodated in the clinic. The system is affixed to the forearm to facilitate image registration, such that a simple ink spot in the ROI or indigenous markers such as skin microvasculature were sufficient to align images to correct for participant movement. As a result, it was straightforward to resolve the same microvasculature over time, and even track the same individual vessels.

To the best of our knowledge, these experiments are the first report of the use of optoacoustics for measuring changes in vascular response to external stimuli in real time at the level of individual vessels. The results highlight the impressive potential of RSOM for basic and clinical investigations, but the method could still be improved. Each image obtained in these experiments required 40 s of scanning, which should be reduced in order to resolve rapid microvasculature processes and to improve the accuracy of blood volume and vessel diameter measurements during the early stages of dilation. Nevertheless, the current system was able to measure large increases in blood volume, in agreement with previous reports based on optical measurements [15].

In summary, the assessment of hyperemic response in human skin using noninvasive clinical RSOM system shown here suggests vast, previously unrecognized possibilities for physiological measurements of thermoregulatory function of skin and imaging of cutaneous microcirculation. Further work will help to elucidate the physiological mechanism involved in the perfusion changes that can be captured with RSOM. We strongly believe that future work not only will focus on vasodilation but also on vasoconstriction effect analyses, with changes in blood oxygenation induced by various stimuli providing major insights in the biology and physiology of the skin. We anticipate that the presented method will allow elucidation of thermoregulatory vascular processes that remain poorly understood [34] and that may be useful for diagnosis and monitoring of major diseases.

ACKNOWLEDGMENTS

This study has received funding by in part by the European Union's Horizon 2020 research and innovation programme under grant agreement no. 687866 (INNODERM), funding from the European Research Council (ERC) through the European Union's Horizon 2020 research and innovation programme under grant agreement no. 694968 (PREMSOT). A.B. thanks all the participants for taking part in the measurements and Chapin Rodriguez for proofreading the manuscript.

AUTHOR BIOGRAPHIES

Please see Supporting Information online.

REFERENCES

[1] C. T. Minson, *J. Appl. Physiol.* **2010**, *109*(4), 1239.
[2] R. Joannides, J. Bellien, C. Thuillez, *Fundam. Clin. Pharmacol.* **2006**, *20*(3), 311.
[3] L. A. Holowatz, C. S. Thompson-torgerson, W. L. Kenney, *J. Appl. Physiol.* **2008**, *105*(1), 370.
[4] I. Fredriksson, M. Larsson, F. H. Nyström, T. Länne, C. J. Östgren, T. Strömberg, *Diabetes* **2010**, *59*(7), 1578.
[5] C. Freccero, H. Svensson, S. Bornmyr, P. Wollmer, G. Sundkvist, *Diabetes Care* **2004**, *27*(12), 2936.
[6] J. C. Patik, K. M. Christmas, C. Hurr, R. M. Brothers, *Microvasc. Res.* **2016**, *104*, 63.
[7] J. Cui, A. Arbab-Zadeh, A. Prasad, S. Durand, B. D. Levine, C. G. Crandall, *Circulation* **2005**, *112*(15), 2286.
[8] D. J. Green, A. J. Maiorana, J. H. J. Siong, V. Burke, M. Erickson, C. T. Minson, W. Bilsborough, G. O'Driscoll, *Eur. Heart J.* **2006**, *27*(3), 338.

[9] L. Jayakody, T. Kappagoda, M. P. J. Senaratne, A. B. R. Thomson, *Br. J. Pharmacol.* **1988**, *94*(2), 335.
[10] L. G. Kraemer-Aguiar, C. M. Laflor, E. Bouskela, *Metabolism* **2008**, *57*(12), 1740.
[11] J. M. Johnson, C. T. Minson, D. L. Kellogg, *Compr. Physiol.* **2014**, *4*(1), 33.
[12] D. L. Kellogg, *J. Appl. Physiol.* **2006**, *100*(5), 1709.
[13] R. B. D'Agostino, R. S. Vasan, M. J. Pencina, P. A. Wolf, M. Cobain, J. M. Massaro, W. B. Kannel, *Circulation* **2008**, *117*(6), 743.
[14] R. Bonner, R. Nossal, *Appl. Optics* **1981**, *20*(12), 2097.
[15] C. Song, L. Chelstrom, D. Aumschild, D. Haumschild, D. Aumschild, *Int. J. Radiat. Oncol. Biol. Phys.* **1990**, *18*(4), 903.
[16] D. J. Haumschild, C. W. Song, L. M. Chelstrom, S. H. Levitt, *Int. J. Radiat. Oncol. Biol. Phys.* **1989**, *17*(5), 1041.
[17] H. N. Mayrovitz, J. A. Leedham, *Microvasc. Res.* **2001**, *62*(1), 74.
[18] M. Roustit, C. Millet, S. Blaise, B. Dufournet, J. L. Cracowski, *Microvasc. Res.* **2010**, *80*(3), 505.
[19] T. Binzoni, P. A. a Humeau-Heurtier, G. Mahe, *IEEE Trans. Biomed. Eng.* **2013**, *60*(5), 1259.
[20] T. Durduran, A. G. Yodh, *Neuroimage* **2014**, *85*(1), 51.
[21] C. Zhou, G. Yu, D. Furuya, J. H. Greenberg, A. G. Yodh, T. Durduran, *Opt. Express* **2006**, *14*(3), 1125.
[22] H. M. Varma, C. P. Valdes, A. K. Kristoffersen, J. P. Culver, T. Durduran, *Biomed. Opt. Express* **2014**, *5*(4), 1275.
[23] M. Omar, D. Soliman, J. Gateau, V. Ntziachristos, *Opt. Lett.* **2014**, *39*(13), 3911.
[24] J. Aguirre, M. Schwarz, D. Soliman, A. Buehler, M. Omar, V. Ntziachristos, *Opt. Lett.* **2014**, *39*(21), 6297.
[25] M. Schwarz, M. Omar, A. Buehler, J. Aguirre, V. Ntziachristos, *IEEE Trans. Med. Imaging* **2015**, *34*(2), 672.
[26] I. M. Braverman, *Microcirculation* **1997**, *4*(3), 329.
[27] J. Aguirre, M. Schwarz, N. Garzorz, M. Omar, A. Buehler, K. Eyerich, V. Ntziachristos, *Nat. Biomed. Eng.* **2017**, *1*(1), 1.
[28] M. Schwarz, A. Buehler, J. Aguirre, V. Ntziachristos, *J. Biophotonics* **2016**, *9*(1–2), 55.
[29] V. Ntziachristos, *Nat. Methods* **2010**, *7*(8), 603.
[30] M. Omar, J. Gateau, V. Ntziachristos, *Opt. Lett.* **2013**, *38*(14), 2472.
[31] J. Turner, H. Estrada, M. Kneipp, D. Razansky, *Opt. Lett.* **2014**, *39*(12), 3390.
[32] H. Barcroft, O. G. Edholm, *J. Physiol.* **1943**, *102*(1), 5.
[33] G. Mahé, A. Humeau-Heurtier, S. Durand, G. Leftheriotis, P. Abraham, *Circ. Cardiovasc. Imaging* **2012**, *5*(1), 155.
[34] C. T. Minson, L. T. Berry, M. J. Joyner, *J. Appl. Physiol.* **2013**, *97403*, 1619.

SUPPORTING INFORMATION

Additional Supporting Information may be found online in the supporting information tab for this article.

Appendix S1. RSOM system, image reconstruction and representation

How to cite this article: Berezhnoi A, Schwarz M, Buehler A, Ovsepian SV, Aguirre J, Ntziachristos V. Assessing hyperthermia-induced vasodilation in human skin in vivo using optoacoustic mesoscopy. *J. Biophotonics*. 2018;11:e201700359. https://doi.org/10.1002/jbio.201700359